Nonlinear Radiation and Variable Viscosity Effects on Free Convection of a Power-Law Nanofluid Over a Truncated Cone in Porous Media With Zero Nanoparticles Flux and Internal Heat Generation

Chuo-Jeng Huang
Department of Aircraft Engineering,
Air Force Institute of Technology,
Kaohsiung City 82063, Taiwan (ROC)
e-mail: hcj631216@yahoo.com.tw

Kuo-Ann Yih
Department of Aircraft Engineering,
Air Force Institute of Technology,
Kaohsiung City 82063, Taiwan (ROC)
e-mail: chhsingy@gmail.com

This study used numerical analysis to investigate the effects of nonlinear radiation and variable viscosity on free convection of a power-law nanofluid over a vertical truncated cone in porous media with Rosseland diffusion approximation considering zero nanoparticles flux and internal heat generation. The internal heat generation is of an exponential decaying form and the viscosity of the fluid is assumed to follow Reynolds viscosity model. The surface boundary conditions of vertical truncated cone is maintained at the uniform wall temperature (UWT) and the zero nanoparticle flux (ZNF) to cause the results to be more realistic and useful. The nanofluid model considered the effects of Brownian motion and thermophoresis. The nonsimilar governing equations are obtained by using a suitable coordinate transformation and then solved by Keller box method (KBM). Comparisons with previously published work obtained good agreement. Graphical and tabular presentations of numerical data for the dimensionless temperature profile and the local Nusselt number were presented for main parameters: dimensionless streamwise coordinate, thermophoresis parameter, Lewis number, radiation parameter, surface temperature parameter, viscosity parameter, power-law index of the non-Newtonian fluid, and internal heat generation coefficient. The local Nusselt number increased when the following parameters were increased: radiation parameter, surface temperature parameter, viscosity parameter, power-law index of the non-Newtonian fluid, and dimensionless streamwise coordinate. In contrast, the local Nusselt number decreased when the following parameters were increased: internal heat generation coefficient, thermophoresis parameter, and Lewis number. Besides, the physical aspects of the problem are discussed in details. [DOI: 10.1115/1.4048453]

Keywords: zero nanoparticles flux, natural convection, vertical truncated cone, porous media, nanofluid, heat and mass transfer, natural and mixed convection

Introduction

The study of convective heat and mass transfer in a saturated porous medium has important applications such as geothermal reservoirs, nuclear reactor cooling system, and underground disposal of nuclear wastes. A recent monograph by Nield and Bejan [1] comprehensively discussed the available information in this field. Concerning the aspect of pure heat transfer in porous media, Cheng et al. [2] first studied natural convection of a Darcian fluid about a vertical full core by similarity solution or truncated cone by local nonsimilarity solution. Chamkha [3] studied non-Darcy hydromagnetic free convection from a cone and a wedge in porous media. Chamkha et al. [4] performed a numerical analysis of free convection flow over a truncated cone embedded in a porous medium saturated with pure or saline water at low temperatures. Regarding combined heat and mass transfer, Yih [5] extended the work of Cheng et al. [2] to analyze the double-diffusion from a vertical truncated cone with the both variable wall temperature/concentration (VWT/VWC) and variable heat/mass flux (VHF/VMF) boundary conditions in a saturated porous medium using Keller box method (KBM). An integral method for heat and mass transfer by free convection from a vertical VWT/VWC truncated cone with in porous media was presented by Cheng [6]. Takhar et al. [7] investigated combined heat and mass transfer along a vertical moving cylinder with a free stream. Hydromagnetic combined heat and mass transfer by natural convection from a permeable surface embedded in a fluid-saturated porous medium was analyzed by Chamkha and Khaled [8]. Takhar et al. [9] presented unsteady mixed convection flow from a rotating vertical cone with a magnetic field. Later, Cheng [10] extended the research of Yih [5] to examine Soret and Dufour effects on heat and mass transfer by natural convection from a vertical VWT/VWC truncated cone in porous media by the cubic spline collocation method.

Numerous industrially important fluids present the behavior of non-Newtonian. The convection flow of non-Newtonian fluids in a saturated porous medium is extremely important because of its engineering applications, e.g., oil recovery and food processing. As for the study of non-Newtonian fluids in a porous medium, Chen and Chen [11] investigated free convection flow of non-Newtonian fluids along a vertical plate. Boundary-layer flow and heat transfer of non-Newtonian fluids in porous media was studied by Wang and Tu [12]. Yih [13] extended the work of Chen and Chen [11] to examine uniform lateral mass flux effect

Manuscript received March 9, 2020; final manuscript received August 10, 2020; published online November 6, 2020. Assoc. Editor: Sandip Mazumder.

on free convection of non-Newtonian fluids over the vertical plate and cone in porous media by utilizing KBM. Cheng [14] presented natural convection heat transfer of non-Newtonian fluids in porous media from a vertical cone under mixed thermal boundary conditions by the cubic spline collocation method. Free convection of coupled heat and mass transfer about a vertical truncated cone in a porous medium saturated with a non-Newtonian fluid was studied by Cheng [15] for the VWT/VWC case.

The internal heat generation effect must be considered in reactor safety analysis, fire and combustion studies, and the storage of radioactive materials. Regarding research in the internal heat generation effect in a porous medium, natural convection in non-Newtonian fluid-saturated porous media with an exponential decaying internal heat generation was investigated over a vertical flat plate in Groşan and Pop [16] and over a vertical cone in Groşan et al. [17]. The similarity equations are solved numerically using a version of the shooting method. Chamkha and Al-Mudhaf [18] presented unsteady heat and mass transfer from a rotating vertical cone with a magnetic field and heat generation or absorption effects. Al-Mudhaf and Chamkha [19] studied similarity solutions for magnetohydrodynamic (MHD) thermosolutal Marangoni convection over a flat surface considering heat generation or absorption effects. The effect of heat generation or absorption on thermophoretic free convection boundary layer from a vertical flat plate embedded in a porous medium was investigated by Chamkha et al. [20]. Damseh et al. [21] analyzed the combined effects of heat generation or absorption and first-order chemical reaction on micropolar fluid flows over a uniformly stretched permeable surface. Khedr et al. [22] examined MHD flow of a micropolar fluid past a stretched permeable surface with heat generation or absorption. A full analytical solution for the combined effect of heat generation or absorption and first-order chemical reaction on micropolar fluid flows over a uniformly stretched permeable surface was reported in Magyari and Chamkha [23]. An analytical solution for natural convection past a vertical cone in a non-Newtonian fluid-saturated porous medium with internal heat generation effect was reported in Rashidi and Rastegari [24]. The similarity equations are solved analytically using a homotopy analysis method. Recently, Yih and Huang [25,26] analyzed internal heat generation effect on natural convection heat and mass transfer of non-Newtonian fluids flow over a vertical plate [25] and a vertical truncated cone [26] in porous media for the case of VWT/VWC. Huang [27] examined internal heat generation and Soret/Dufour effects on natural convection of non-Newtonian fluids about a vertical permeable cone in porous media.

The effect of radiation on convection flow has many important applications, including space technology and processes involving high temperatures, e.g., geothermal engineering and nuclear reactor cooling systems. Chamkha [28] analyzed solar radiation-assisted convection in uniform porous medium supported by a vertical flat plate. Coupled heat and mass transfer by natural convection about a truncated cone in the presence of magnetic and radiation effects were presented by Chamkha [29]. Unsteady MHD natural convection from a heated vertical porous plate in a micropolar fluid with Joule heating, chemical reaction, and radiation effects was investigated by Chamkha et al. [30]. Yih [31] used the Rosseland diffusion approximation to extend the work of Cheng et al. [2] in an analysis of the effect of thermal radiation on combined free and forced convection over an isothermal cone in porous media. In an extension of the work of Groşan et al. [17], Mahmoud [32] presented the effect of thermal radiation on natural convection of a non-Newtonian fluid about a vertical cone embedded in a porous medium in the presence of exponentially decaying internal heat generation. Recently, Huang [33,34] extended the work of Mahmoud [32] and used the KBM to investigate numerically the Soret/Dufour effects on coupled heat and mass transfer by free convection over a vertical cone with internal heat generation and thermal radiation influences [33] and uniform blowing/suction and thermal radiation effects [34] in porous media, respectively. To simplify their analysis, articles [32–34] assumed that, because of the small temperature difference within the flow, may be expressed as $T^4 = 4T_\infty^3 T - 3T_\infty^4$ (linear function of temperature T) by a Taylor series expansion about T_∞ and neglecting higher-order terms. In the energy equation in Ref. [31], however, the term T^4 (nonlinear) is retained.

In the above studies [2–34], fluid viscosity was assumed to be constant. However, viscosity is known to change significantly with temperature. Therefore, in order to predict the fluid flow behavior accurately, it is necessary to consider the viscosity variation. In the aspect of variable viscosity effect on heat transfer in a porous medium, Gary et al. [35] described how large viscosity changes affect convective heat transfer transport in water-saturated porous medium. Bagai [36] used the Reynolds viscosity model to solve the problem of effect of variable viscosity on free convection over a nonisothermal axisymmetric body in a porous medium with internal heat generation (the viscosity decreases exponentially with temperature). Kairi et al. [37] presented the effect of viscous dissipation on natural convection in a non-Darcy porous medium saturated with non-Newtonian fluid of variable viscosity. Bagai and Nishad [38] extended the work of Bagai [36] by analyzing the effect of variable viscosity on free convective heat transfer over a non-isothermal body with an arbitrary shape in a non-Newtonian fluid-saturated porous medium considering internal heat generation. They observed that the heat transfer rate increases for a less viscous fluid. The effects of viscosity and fluid suction/injection on free convection flow from a vertical plate in a porous medium saturated with a pseudo-plastic fluid were studied by Achemlal et al. [39]. In the couple heat and mass transfer aspect, Cheng [40] examined nonsimilar boundary layer analysis of double-diffusive convection from a vertical truncated cone in a porous medium with variable viscosity. Mahdy et al. [41] extended Cheng [40] by including magnetic field and radiation effects. Narayana et al. [42] analyzed the Soret effect on the natural convection from a vertical plate in a thermally stratified porous medium saturated with non-Newtonian liquid.

Nanotechnology applications have been reported in the biological sciences, physical sciences, electronic cooling, and advanced nuclear systems. The term "nanofluid" refers to a liquid containing a suspension of submicronic solid particles (nanoparticles). The heat transfer characteristic of nanofluid is very important because these fluids may be applicable for increasing the heat transfer rate. Buongiorno [43] comprehensively surveyed convection in nanofluids and derived the conservation equations for nanofluids involving both the Brownian motion and thermophoresis effects. Recently, Kakaç and Pramuanjaroenkij [44] and Mahdi et al. [45] reviewed the literature on convection heat transfer and fluid flow in porous media with nanofluid. The following studies are the most important numerical studies of nanofluids convective boundary-layer flow in porous media filled with a nanofluid. Nield and Kuznetsov [46] used the Buongiorno nanofluid model to study the Cheng-Minkowycz problem for natural convective boundary-layer flow in a porous medium saturated by a nanofluid. Cheng investigated natural convection boundary-layer flow over a truncated cone in a porous medium saturated by Newtonian nanofluids in Ref. [47] and by non-Newtonian nanofluids in Ref. [48], respectively. Rashad et al. [49] extended the work of Yih [13] in a study of natural convection boundary layer of a non-Newtonian fluid about a permeable vertical cone in porous media saturated with a nanofluid. The effects of heat generation/absorption on natural convective boundary-layer flow from a vertical cone embedded in a porous medium filled with a non-Newtonian nanofluid were analyzed by Hady et al. [50]. Chamkha et al. [51] presented the effect of suction/injection on free convection along a vertical plate in a nanofluid saturated non-Darcy porous medium with internal heat generation. Chamkha et al. [52] extended the research of Yih [31] by examining the nonlinear effects of thermal radiation on mixed convection about a cone embedded in a porous medium filled with a nanofluid. Recently, variable viscosity effect on non-aligned MHD stagnation point flow of nanofluids past a stretching sheet with radiative heat was presented by Khan et al. [53].

However, the model in the above articles [46–53] controlled for nanoparticle volume fraction at the boundary. Therefore, Kuznetsov and Nield [54] developed a revised model and repeated the experiments in Nield and Kuznetsov [46] for natural convective boundary-layer flow in a porous medium saturated by a nanofluid. In their revised model, the nanoparticle volume fraction on the boundary is passively rather than actively controlled, i.e., the zero nanoparticle flux (ZNF), leading the solutions to be more realistic and useful. They observed that the Nusselt number decreases independently of the Brownian motion parameter, which is different from the results of Nield and Kuznetsov [46]. Cheng [55] also used the revised model to study free convection about a vertical full cone in a porous medium saturated by a nanofluid. Brownian motion parameter and the buoyancy ratio had almost no effect on the local Nusselt number. However, increasing the thermophoresis parameter decreases the local Nusselt number. The problem of MHD boundary-layer flow of a power-law nanofluid with new mass flux condition was solved by Khan and Khan [56]. Khan et al. [57] investigated the triple convective-diffusion boundary layer along a vertical flat plate in a porous medium saturated by a water-based nanofluid. Kameswaran et al. [58] solved the problem of mixed convection from a wavy surface embedded in a thermally stratified nanofluid saturated porous medium with nonlinear Boussinesq approximation. Gorla and Chamkha [59] studied natural convective boundary-layer flow over a nonisothermal vertical plate embedded in a porous medium saturated with a nanofluid. RamReddy et al. [60] examined the Soret effect on mixed convection flow in a nanofluid under the condition of a convective boundary. Ghalambaz et al. [61] analyzed effects of nanoparticles diameter and concentration on natural convection of the Al_2O_3–water nanofluids considering variable thermal conductivity around a vertical cone in porous media. Sudarsana Reddy and Chamkha [62] studied Soret and Dufour effects on MHD convective flow of Al_2O_3–water and TiO_2–water nanofluids past a stretching sheet in porous media with heat generation/absorption. The MHD boundary-layer flow, heat and mass transfer analysis over a rotating disk and through a porous medium saturated with Cu-water and Ag-water nanofluid with chemical reaction was presented by Reddy et al. [63]. Rasool et al. [64] studied entropy generation and consequences of binary chemical reaction on MHD Darcy-Forchheimer Williamson nanofluid flow over nonlinearly stretching surface.

Therefore, the objective of the present work was to extend works by Cheng et al. [2], Groşan et al. [17], Bagai and Nishad [38], Cheng [48], Chamkha et al. [52], and Cheng [55] by using the Reynolds viscosity model to investigate the effects of nonlinear thermal radiation and variable viscosity on natural convection of a power-law nanofluid over a vertical truncated cone in porous media with zero nanoparticles flux and exponential decaying internal heat generation. The governing numerical equations were solved by KBM. The results are obtained and discussed for various values of the main parameters in tabular and graphic forms.

Analysis

Consider the problem of the influences of zero nanoparticles flux, internal heat generation, nonlinear radiation, and variable viscosity on free convection of a non-Newtonian nanofluid past a vertical truncated cone (with half angle γ) embedded in a fluid-saturated porous medium filled with a nanofluid. Figure 1 illustrates the flow model and physical coordinate system. The origin of the coordinate system is placed at the vertex of the full cone, where x is the coordinate along the surface of cone measured from the origin and y is the coordinate normal to the surface, respectively. r is the local radius of the vertical truncated cone. The x_o is the distance from the origin to the leading edge of the vertical truncated cone. The boundary conditions are maintained at the UWT T_w and ZNF; T_w is higher than the ambient temperature T_∞. C_∞ is the ambient nanoparticle volume fraction. g is the gravitational acceleration.

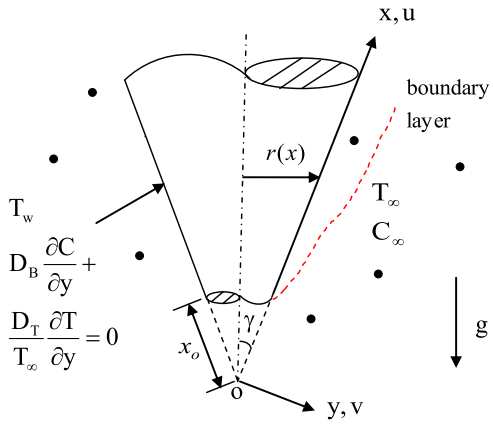

Fig. 1 Flow model and physical coordinate system

The effects of Brownian motion and thermophoresis on the nanofluids are also incorporated into the model. All the fluid properties are assumed to be constant except for the viscosity of fluid and the density variation in the buoyancy term. The viscous dissipation effect is neglected for the low velocity.

For the boundary layer and Oberbeck–Boussinesq approximations, the governing equations and the boundary conditions based on the Darcy law [48,52,55] can be written as follows:

Conservation of mass:

$$\frac{\partial(ru)}{\partial x}+\frac{\partial(rv)}{\partial y}=0 \tag{1}$$

Conservation of momentum:

$$\frac{\partial u^n}{\partial y}=\frac{g\cos\gamma K}{\mu}\left[(1-C_\infty)\rho_{f\infty}\beta\frac{\partial T}{\partial y}-(\rho_p-\rho_{f\infty})\frac{\partial C}{\partial y}\right] \tag{2}$$

Conservation of energy:

$$u\frac{\partial T}{\partial x}+v\frac{\partial T}{\partial y}=\alpha\frac{\partial^2 T}{\partial y^2}+\frac{q'''}{(\rho c)_f}+\frac{16\sigma_o}{3(a_r+\sigma_s)(\rho c)_f}\frac{\partial}{\partial y}\left(T^3\frac{\partial T}{\partial y}\right)+\tau\left[D_B\frac{\partial C}{\partial y}\frac{\partial T}{\partial y}+\left(\frac{D_T}{T_\infty}\right)\left(\frac{\partial T}{\partial y}\right)^2\right] \tag{3}$$

Conservation of nanoparticles:

$$u\frac{\partial C}{\partial x}+v\frac{\partial C}{\partial y}=D_B\frac{\partial^2 C}{\partial y^2}+\left(\frac{D_T}{T_\infty}\right)\frac{\partial^2 T}{\partial y^2} \tag{4}$$

Boundary conditions:

$$y=0:\quad v=0,\quad T=T_w,\quad D_B\frac{\partial C}{\partial y}+\frac{D_T}{T_\infty}\frac{\partial T}{\partial y}=0 \tag{5}$$

$$y\to\infty:\quad u=0,\quad T=T_\infty,\quad C=C_\infty \tag{6}$$

Here, u and v denote the volume-averaged velocity components in the x- and y-directions, respectively. The T is the volume-averaged temperature. The C is the nanoparticle volume fraction. The $K(n)$ is the modified permeability of the porous medium. n is the power-law index of the non-Newtonian fluid; ρ_f, μ, and β are the density, viscosity, and volumetric expansion coefficient of the fluid. The ρ_p is the density of the nanoparticle. α is the thermal diffusivity of the porous medium. The heat capacity ratio between nanoparticle and fluid is defined as $\tau=(\rho c)_p/(\rho c)_f$. $(\rho c)_p$ and $(\rho c)_f$ are the effective heat capacity of the nanoparticle material and the heat capacity of the fluid, respectively. c is the specific heat at constant pressure. q''' is the internal heat generation rate per unit volume; σ_o, a_r, and σ_s are the Stefan-Boltzmann constant, the Rosseland mean extinction

coefficient, and the scattering coefficient, respectively. The D_B and D_T are the Brownian diffusion coefficient and the thermophoresis diffusion coefficient, respectively. The third term of Eq. (5) is the ZNF. Hence, the nanoparticle volume fraction on the boundary is passively controlled.

Since the boundary layer is sufficiently thin in comparison with the local radius of the vertical truncated cone. The local radius to a point in the boundary layer, therefore, can be replaced by the radius of the vertical truncated cone, i.e., $r = x \sin \gamma$. Equations (1)–(6) are valid in $x_o \le x < \infty$.

Christopher and Middleman [65] and Dharmadhikari and Kale [66] proposed the power-law model of modified the power-lawmodel proposed by Ostwald-de-Waele:

$$K(n) = \begin{cases} \dfrac{6}{25}\left(\dfrac{n\varepsilon}{3n+1}\right)^n \left[\dfrac{\varepsilon d}{3(1-\varepsilon)}\right]^{n+1} \\ \dfrac{2}{\varepsilon}\left[\dfrac{d\varepsilon^2}{8(1-\varepsilon)}\right]^{n+1}\left(\dfrac{6n+1}{10n-3}\right)\left(\dfrac{16}{75}\right)^{(3(10n-3))/((10n+11))} \end{cases} \tag{7}$$

where d is the particle diameter while ε is the porosity.

Note that the power-law fluid index $n < 1$ corresponds to pseudoplastic fluids (for example, the polymer solution), $n = 1$ to Newtonian fluids (for instance, air and water), and $n > 1$ to dilatant fluids (for example, the suspensions of sand) [13–15].

The stream function ψ is defined by

$$ru = \partial\psi/\partial y, \quad rv = -\partial\psi/\partial x \tag{8}$$

Therefore, the continuity equation is automatically satisfied.

Invoking the following dimensionless nonsimilarity variables:

$$\xi = \frac{x^*}{x_o} = \frac{x - x_o}{x_o} \tag{9}$$

$$\eta = \frac{y}{x^*}\mathrm{Ra}_{x^*}^{1/(2n)} \tag{10}$$

$$f(\xi, \eta) = \frac{\psi}{\alpha r \mathrm{Ra}_{x^*}^{1/(2n)}} \tag{11}$$

$$\theta(\xi, \eta) = \frac{T - T_\infty}{T_w - T_\infty} \tag{12}$$

$$\varphi(\xi, \eta) = \frac{C - C_\infty}{C_\infty} \tag{13}$$

$$\mathrm{Ra}_{x^*} = \frac{(1 - C_\infty)\rho_{f\infty} g \cos\gamma \beta K (T_w - T_\infty)}{\mu_\infty}\left(\frac{x^*}{\alpha}\right)^n \tag{14}$$

where Ra_{x^*} is the local Rayleigh number for the flow through the porous medium.

The internal heat generation rate per unit volume q''' is modeled according to the exponential decaying form [24–27]:

$$q''' = A^* \frac{k \mathrm{Ra}_{x^*}^{1/n}}{(x^*)^2}(T_w - T_\infty)e^{-\eta} \tag{15}$$

Here, A^* is the internal heat generation coefficient. Note that $A^* = 0$ corresponds to the absence of internal heat generation while $A^* > 0$ corresponds to the presence of internal heat generation. The k is the equivalent thermal conductivity.

The fluid viscosity obeying Reynolds viscosity model [36–39,42] is given by

$$\mu(\theta) = \mu_\infty e^{-\Omega\theta} \tag{16}$$

where μ_∞ is the ambient viscosity of the medium and Ω is the viscosity parameter depending on the nature of the fluid. This model can be applicable in many processes where pre-heating of the fuel is used as a means to enhanced heat transfer effect. For some fluids, such as lubricants, polymers, an appropriate constitutive relation where viscosity is a function of temperature should be used.

Substituting Eqs. (9)–(16) into Eqs. (1)–(6), we obtain

$$(f')^n = e^{\Omega\theta}(\theta - Nr\varphi) \tag{17}$$

$$\theta'' + \left(\frac{\xi}{1+\xi} + \frac{1}{2}\right) f\theta' + A^* e^{-\eta} + \frac{4R_d}{3}\left\{\theta'[(H-1)\theta + 1]^3\right\}' + Nb\varphi'\theta' + Nt(\theta')^2 = \xi\left(f'\frac{\partial\theta}{\partial\xi} - \theta'\frac{\partial f}{\partial\xi}\right) \tag{18}$$

$$\frac{1}{\mathrm{Le}}\varphi'' + \left(\frac{\xi}{1+\xi} + \frac{1}{2}\right) f\varphi' + \frac{1}{\mathrm{Le}}\frac{Nt}{Nb}\theta'' = \xi\left(f'\frac{\partial\varphi}{\partial\xi} - \varphi'\frac{\partial f}{\partial\xi}\right) \tag{19}$$

The boundary conditions are defined as follows:

$$\eta = 0: \quad f = 0, \quad \theta = 1, \quad Nb\,\varphi' + Nt\,\theta' = 0 \tag{20}$$

$$\eta \to \infty: \quad \theta = 0, \quad \varphi = 0 \tag{21}$$

In the above, primes denote differentiation with respect to η. Equation (17) is obtained by integrating Eq. (2) once with the help of Eq. (6).

In addition, in terms of the new variables, the volume-averaged velocities in x- and y-directions are, respectively, given by

$$u = \frac{\alpha \mathrm{Ra}_{x^*}^{1/n}}{x^*} f' \tag{22}$$

$$v = -\frac{\alpha \mathrm{Ra}_{x^*}^{1/(2n)}}{x^*}\left[\left(\frac{\xi}{1+\xi} + \frac{1}{2}\right) f + \xi\frac{\partial f}{\partial\xi} - \frac{1}{2}\eta f'\right] \tag{23}$$

Besides, the important parameters are defined below:

$$R_d = \frac{4\sigma_o T_\infty^3}{k(a_r + \sigma_s)} \tag{24}$$

$$H = \frac{T_w}{T_\infty} \tag{25}$$

$$Nr = \frac{(\rho_p - \rho_{f\infty})C_\infty}{\rho_{f\infty}\beta(T_w - T_\infty)(1 - C_\infty)} \tag{26}$$

$$Nb = \frac{\tau D_B C_\infty}{\alpha} \tag{27}$$

$$Nt = \frac{\tau D_T (T_w - T_\infty)}{T_\infty \alpha} \tag{28}$$

$$\mathrm{Le} = \frac{\alpha}{D_B} \tag{29}$$

Here, R_d, H, Nr, Nb, Nt, and Le denote the radiation parameter, the surface temperature parameter, the buoyancy ratio, the Brownian motion parameter, the thermophoresis parameter, and the Lewis number, respectively.

In practice, the most important result is the surface heat transfer rate. The surface heat transfer rate is expressed in terms of the local Nusselt number Nu_{x^*}, which is defined as follows:

$$\mathrm{Nu}_{x*} = \frac{h_{x^*}x^*}{k} = \frac{q_w x^*}{(T_w - T_\infty)k} \tag{30}$$

where h_{x^*} is the local convective heat transfer coefficient and the local heat flux $q_w = h_{x^*}(T_w - T_\infty)$ (Newton law of cooling).

Table 1 Comparison of the values of $-\theta'(\xi, 0)$ for A^* with $Nr = Nt = Nb = 0$, $n = 1$, $R_d = 0$, $\Omega = 0$

	$-\theta'(\xi, 0)$						
	$A^* = 0$					$A^* = 1$	
ξ	Cheng et al. [2]	Chamkha et al. [4]	Yih [5]	Cheng [15]	Present results	Yih and Huang [26]	Present results
0	0.4437	0.4444	0.4439	0.4439	0.4437	−0.2153	−0.2153
0.5	0.5412	0.5294	0.5285	0.5285	0.5286	–	−0.1195
1	0.5991	0.5812	0.5807	0.5807	0.5808	–	−0.0557
2	0.6572	0.6399	0.6373	0.6373	0.6373	–	0.0165
6	0.7219	0.7130	0.7123	0.7116	0.7123	–	0.1176
10	0.7391	0.7336	0.7330	0.7326	0.7330	–	0.1463
20	0.7532	0.7507	0.7500	0.7490	0.7500	–	0.1700
40	0.7607	0.7596	0.7592	0.7587	0.7591	–	0.1827
∞	0.7685	0.7690	0.7686	0.7686	0.7685	0.1957	0.1957

$\xi \to \infty$: denotes $\xi = 10^4$.

According to the Fourier law of heat conduction and the Rosseland diffusion approximation, the rate of surface heat transfer q_w is defined as follows:

$$q_w = q_{cond} + q_r = -k\left(\frac{\partial T}{\partial y}\right)\Big|_{y=0} - \frac{16\sigma_0 T^3}{3(a_r + \sigma_s)}\left(\frac{\partial T}{\partial y}\right)\Big|_{y=0} = -\left\{\left[k + \frac{16\sigma_0 T^3}{3(a_r + \sigma_s)}\right]\right\}\left(\frac{\partial T}{\partial y}\right)\Big|_{y=0} \tag{31}$$

Inserting Eq. (31) into Eq. (30) and with the aid of Eqs. (9)–(14), the local Nusselt number

Nu_{x^*} in terms of $\mathrm{Ra}_{x^*}^{1/(2n)}$ is obtained by

$$\frac{\mathrm{Nu}_{x^*}}{\mathrm{Ra}_{x^*}^{1/(2n)}} = -\left(1 + \frac{4}{3}R_d H^3\right)\theta'(\xi, 0) \tag{32}$$

However, as $Nr = 0$ (pure heat transfer), $n = 1$, $Nt = Nb = R_d = A^* = \Omega = 0$, Eqs. (17) and (18), (20) and (21) are reduced as described in Cheng et al. [2] where a nonsimilar solution was obtained before. (The boundary value problem for φ then becomes ill-posed and is of no physical significance.) When $A^* = 1$, $\xi = \gamma = 0$ ($\xi \to \infty$), i.e., vertical flat plate (vertical cone), Eqs. (17) and (18), (20) and (21) are reduced as reported previously in Groşan and Pop [16] (Groşan et al. [17]) where similar solutions were obtained previously. However, in the case of $n = 1$, $R_d = A^* = \Omega = 0$, and $\xi = \gamma = 0$ ($\xi \to \infty$), Eqs. (17)–(21) are reduced to those of Kuznetsov and Nield [54] (Cheng [55]) where a similar solution was obtained previously.

Numerical Method

This analysis integrates Eqs. (17)–(21) by using the implicit finite difference approximation and the Keller box method developed by Cebeci and Bradshaw [67]. First, differential equations are converted into a system of five first-order equations. These first-order equations are expressed in finite difference forms, and the equations and their boundary conditions are then solved by an iterative

Table 2 Comparison of the values of $-\theta'(0, 0)$ (vertical plate) for A^* with $Nr = Nt = Nb = 0$, $n = 1$, $R_d = 0$, $\Omega = 0$

	$-\theta'(0, 0)$ (vertical plate)								
	$A^* = 0$						$A^* = 1$		
n	Chen and Chen [11]	Wang and Tu [12]	Groşan and Pop [16]	Cheng [48]	Present results	Groşan and Pop [16]	Achemlal et al. [39]	Hady et al. [50]	Present results
0.5	0.3768	–	0.3777	0.3771	0.3765	−0.2754	−0.2755	−0.2754	−0.2756
0.8	0.4238	0.424	0.4240	0.4240	0.4237	−0.2288	−0.2288	−0.2288	−0.2290
1.0	0.4437	0.444	0.4439	0.4439	0.4437	−0.2152	−0.2152	−0.2152	−0.2153
1.5	0.4752	0.475	0.4754	0.4755	0.4754	−0.1921	–	−0.1921	−0.1923
2.0	0.4938	–	0.4938	0.4938	0.4938	−0.1778	–	–	−0.1780

Table 3 Comparison of the values of $-\theta'(\infty, 0)$ (vertical cone) for n and A^* with $Nr = Nt = Nb = 0$, $n = 1$, $R_d = 0$, $\Omega = 0$

	$-\theta'(\infty, 0)$ (vertical cone)								
	$A^* = 0$						$A^* = 1$		
n	Groşan et al. [17]	Cheng [14]	Rashad et al. [49]	Mahmoud [32]	Huang [34]	Present results	Groşan et al. [17]	Hady et al. [50]	Present results
0.5	0.6527	0.6521	0.6522	0.6527	0.6521	0.6521	0.0939	0.0939	0.0931
0.8	0.7340	0.7339	0.7339	0.7339	0.7338	0.7338	0.1646	0.1647	0.1641
1.0	0.7686	0.7686	0.7686	0.7686	0.7685	0.7685	0.1962	0.1962	0.1957
1.5	0.8233	0.8233	0.8233	0.8233	0.8232	0.8233	0.2477	0.2478	0.2473
2.0	0.8552	0.8552	0.8552	0.8552	0.8552	0.8552	0.2787	–	0.2783

Table 4 Comparison of the values of $Nu_{x^*}/Ra_{x^*}^{1/(2n)}$ for R_d, H, A^*, and ξ with $Nr = Nt = Nb = 0$, $n = 1$, $\Omega = 0$

		$Nu_{x^*}/Ra_{x^*}^{1/(2n)}$						
		$A^* = 0$				$A^* = 1$		
				$\xi \to \infty$: vertical cone				
R_d	H	$\xi = 0$: vertical plate Present results	$\xi = 1$ Present results	Chamkha et al. [52]	Present results	$\xi = 0$: vertical plate Present results	$\xi = 1$ Present results	$\xi \to \infty$: vertical cone Present results
0.5	1.1	0.5993	0.7843	1.0380	1.0379	−0.1163	0.0952	0.4095
5	1.1	1.3486	1.7651	2.3359	2.3358	0.5107	0.9542	1.5714
5	2	2.6824	3.5107	4.6461	4.6458	1.7748	2.6249	3.7924
5	3	4.5757	5.9896	7.9256	7.9258	3.6324	5.0604	7.0181
10	3	6.4553	8.4493	11.1814	11.1811	5.4965	7.5008	10.2489

Table 5 Comparison of the values of $-\theta'(0, 0)$ (vertical plate) for Ω and n with $Nr = Nt = Nb = 0$, $R_d = 0$, $A^* = 1$

	$-\theta'(0, 0)$ (vertical plate)						
	$n = 0.5$		$n = 1$			$n = 2$	
Ω	Bagai and Nishad [38]	Present results	Bagai [36]	Bagai and Nishad [38]	Present results	Bagai and Nishad [38]	Present results
0	−0.2574	−0.2576	−0.2152	−0.2152	−0.2153	−0.1780	−0.1780
0.1	−0.2090	−0.2091	−0.19	−0.1891	−0.1892	−0.1644	−0.1644
0.2	−0.1586	−0.1587	−0.16	−0.1625	−0.1626	−0.1507	−0.1507
0.5	0.0070	0.0070	−0.08	−0.0791	−0.0792	−0.1086	−0.1086
0.75	0.1659	0.1658	−0.0055	−0.0053	−0.0054	−0.0725	−0.0725

scheme. This approach gives a better rate of convergence and reduces the numerical computational times.

Computations were performed on a personal computer with $\Delta\xi = 0.001 (0 \le \xi \le 0.01)$, $\Delta\xi = 0.01 (0.01 \le \xi \le 0.1)$, $\Delta\xi = 0.1 (0.1 \le \xi \le 1)$, $\Delta\xi = 1 (1 \le \xi \le 10)$, $\Delta\xi = 10 (10 \le \xi \le 100)$, $\Delta\xi = 100 (100 \le \xi \le 1000)$, $\Delta\xi = 1000 (1000 \le \xi \le 10000)$ in ξ-direction. The first step size $\Delta\eta_1 = 0.01$ and the variable grid parameter is 1.01 in η-direction. The value of boundary-layer edge η_∞ is adjusted for R_d, H, Ω, and n. When the errors in computing the dimensionless wall temperature gradient θ'_w and the dimensionless wall nanoparticle volume fraction φ_w in the next procedure become less than 10^{-5}, the iterative procedure is stopped to give the final dimensionless temperature and nanoparticle volume fraction profiles.

Results and Discussion

The accuracy of the method was verified by comparing the results with those of Cheng et al. [2], Chamkha et al. [4], Yih [5], Cheng [15], Yih and Huang [26], Chen and Chen [11], Wang and Tu [12], Groşan and Pop [16], Cheng [48], Achemlal et al. [39], Hady et al. [50], Groşan et al. [17], Cheng [14], Rashad et al. [49], Mahmoud [32], Huang [34], Chamkha et al. [52], Bagai and Nishad [38], Bagai [36], and Kuznetsov and Nield [54]. Table 1 compares the values of $-\theta'(\xi, 0)$ for A^* with $Nr = Nt = Nb = 0$, $n = 1$, $R_d = 0$, $\Omega = 0$. Tables 2 and 3 compare the values of (a) $-\theta'(0, 0)$ (vertical plate), (b) $-\theta'(\infty, 0)$ (vertical cone) for A^* with $Nr = Nt = Nb = 0$, $n = 1$, $R_d = 0$, $\Omega = 0$, respectively. Table 4 compares the values of $Nu_{x^*}/Ra_{x^*}^{1/(2n)}$ for R_d, H, A^*, and ξ with $Nr = Nt = Nb = 0$, $n = 1$, $\Omega = 0$. Tables 5 and 6 compare the values of (a) $-\theta'(0, 0)$ (vertical plate), (b) $-\theta'(\xi, 0)$ for Ω and n with $Nr = Nt = Nb = 0$, $R_d = 0$, $A^* = 1$, respectively. Table 7 compares the values of $-\theta'(\xi, 0)$ for Nr, Nt, Nb, Le, and A^* with $n = 1$, $\Omega = 0$, $R_d = 0$. Tables 1–7 reveal the excellent agreement obtained for all of the above cases.

Table 6 The values of $-\theta'(\xi, 0)$ for Ω and n with $Nr = Nt = Nb = 0$, $R_d = 0$, $A^* = 1$

	$-\theta'(\xi, 0)$					
	$\xi = 1$			$\xi \to \infty$: vertical cone		
Ω	$n = 0.5$	$n = 1$	$n = 2$	$n = 0.5$	$n = 1$	$n = 2$
0	−0.1233	−0.0557	0.0005	0.0931	0.1957	0.2783
0.1	−0.0678	−0.0257	0.0161	0.1607	0.2323	0.2975
0.2	−0.0096	0.0049	0.0319	0.2322	0.2699	0.3169
0.5	0.1849	0.1016	0.0805	0.4740	0.3890	0.3766
0.75	0.3758	0.1882	0.1224	0.7154	0.4966	0.4283

The local Nusselt number is almost independent of the Brownian motion parameter Nb and the buoyancy ratio Nr [54,55]. Hence, the numerical results are presented for $Nb = Nr = 0.5$ with the dimensionless streamwise coordinate ξ (range, 0–10^4), the thermophoresis parameter Nt (range, 0.1–0.5), the Lewis number Le (range, 10–1000), the radiation parameter R_d (range, 0.5–3), the surface temperature parameter H (range, 1.1–1.5), the viscosity parameter Ω (range, 0–0. 5), the power-law index of the non-Newtonian fluid n (range, 0.5–1.5), and the internal heat generation coefficient A^* (range, 0–1).

Figures 2 and 3 illustrate the effects of two values of the radiation parameter R_d ($R_d = 1$, 3) and the surface temperature parameter H ($H = 1.1$, 1.5) on the dimensionless temperature profile θ and the dimensionless nanoparticle volume fraction profile φ with $Nr = Nb = 0.5$, $Nt = 0.3$, $Le = 10$, $A^* = 1$, $n = 0.5$, $\Omega = 0.2$, $\xi = 1$, respectively. Figure 2 shows that, when both the radiation parameter R_d and the surface temperature parameter H increase, the dimensionless temperature profile becomes wide, but the dimensionless wall temperature gradient $[-\theta'(\xi, 0)]$ becomes narrow. This occurs because the value of R_d or H increases, the radiation absorption in the boundary layer increases, causing the dimensionless temperature profile to become large. However, Fig. 3 shows that the dimensionless nanoparticle volume fraction profile reduces with increasing the radiation parameter and the surface temperature parameter.

Table 8 illustrates the values of the local Nusselt number $Nu_{x^*}/Ra_{x^*}^{1/(2n)}$ for various values of ξ, R_d, and H with $Nr = Nb = 0.5$, $Nt = 0.3$, $Le = 10$, $A^* = 1$, $n = 0.5$, $\Omega = 0.2$. For the fixed

Table 7 Comparison of the values of $-\theta'(\xi, 0)$ for *Nr*, *Nt*, *Nb*, Le, and A^* with $n = 1$, $\Omega = 0$, $R_d = 0$

				$-\theta'(\xi, 0)$						
				$A^* = 0$				$A^* = 1$		
				$\xi = 0$: vertical plate		$\xi = 1$	$\xi \to \infty$: vertical cone	$\xi = 0$: vertical plate	$\xi = 1$	$\xi \to \infty$: vertical cone
Nr	*Nt*	*Nb*	Le	Kuznetsov and Nield [54]	Present results	Present results	Present results	Present results	Present results	Present results
0.1	0.1	0.1	10	0.4334	0.4329	0.5666	0.7498	−0.2260	−0.0683	0.1815
0.1	0.5	0.1	10	0.3914	0.3916	0.5126	0.6783	−0.2679	−0.1180	0.1266
0.5	0.5	0.5	1000	0.3620	0.3643	0.4767	0.6309	−0.2766	−0.1264	0.1128

value of ξ, the local Nusselt number tends to enhance as the radiation parameter R_d and the surface temperature parameter H are increased. In the pure convection heat transfer, the local Nusselt number is only proportional to the dimensionless wall temperature gradient $[-\theta'(\xi, 0)]$. However, Fig. 2 shows that, in the coupled convection and radiation, for the case of large R_d and H (radiation effect becomes significant), although the value of $[-\theta'(\xi, 0)]$ is low, the local Nusselt number is still large. This is because the local Nusselt number is found to be more sensitive to R_d and H than $[-\theta'(\xi, 0)]$, as revealed in Eq. (32). Moreover, when R_d and H are fixed, increasing the dimensionless streamwise coordinate ξ increases the local Nusselt number. Additionally, the local Nusselt number approaches to constant value when ξ is small ($\xi = 0$: vertical flat plate) and large ($\xi \to \infty$: vertical full cone).

Figures 4 and 5 plot the dimensionless temperature profile and the dimensionless nanoparticle volume fraction profile for two values of the thermophoresis parameter Nt ($Nt = 0.1$, 0.5) and the

Table 8 Values of $\mathrm{Nu}_{x^*}/\mathrm{Ra}_{x^*}^{1/(2n)}$ for various values of ξ, R_d, and H with $Nr = Nb = 0.5$, $Nt = 0.3$, Le = 10, $A^* = 1$, $n = 0.5$, $\Omega = 0.2$

	$\mathrm{Nu}_{x^*}/\mathrm{Ra}_{x^*}^{1/(2n)}$					
	$R_d = 1$			$R_d = 3$		
ξ	$H = 1.1$	$H = 1.3$	$H = 1.5$	$H = 1.1$	$H = 1.3$	$H = 1.5$
0	0.0055	0.0912	0.1930	0.3041	0.4920	0.7039
0.001	0.0058	0.0916	0.1935	0.3047	0.4926	0.7047
0.01	0.0092	0.0955	0.1979	0.3098	0.4987	0.7119
0.1	0.0408	0.1323	0.2404	0.3577	0.5560	0.7793
1	0.2449	0.3667	0.5085	0.6600	0.9151	1.2000
10	0.5309	0.6895	0.8731	1.0683	1.3951	1.7586
100	0.5925	0.7586	0.9506	1.1547	1.4962	1.8759
1000	0.5991	0.7660	0.9590	1.1641	1.5071	1.8885
∞	0.5998	0.7668	0.9598	1.1650	1.5082	1.8898

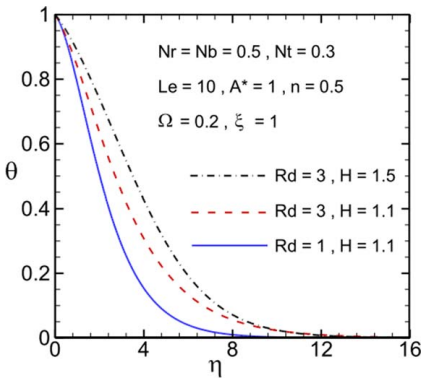

Fig. 2 Dimensionless temperature profile for two values of R_d and H

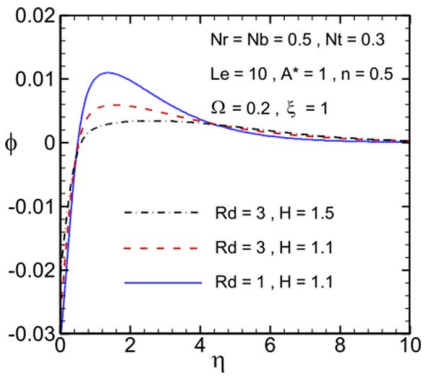

Fig. 3 Dimensionless nanoparticle volume fraction profile for two values of R_d and H

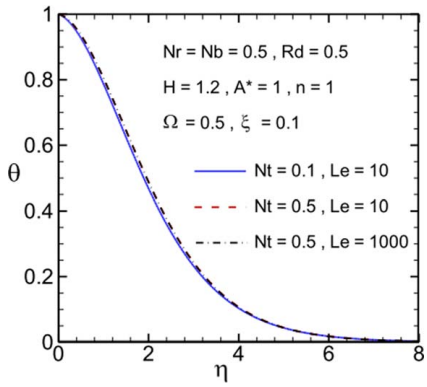

Fig. 4 Dimensionless temperature profile for two values of *Nt* and Le

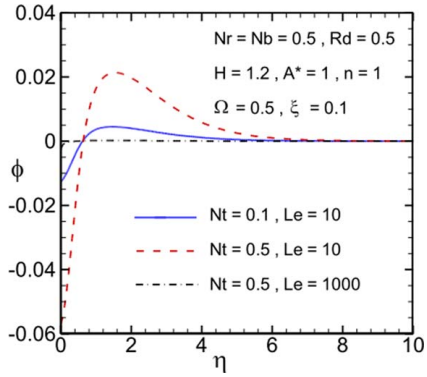

Fig. 5 Dimensionless nanoparticle volume fraction profile for two values of *Nt* and Le

Table 9 Values of $Nu_{x^*}/Ra_{x^*}^{1/(2n)}$ for various values of ξ, Le, and Nt with $Nr = Nb = 0.5$, $R_d = 0.5$, $H = 1.2$, $A^* = 1$, $n = 1$, $\Omega = 0.5$

	$Nu_{x^*}/Ra_{x^*}^{1/(2n)}$					
	Le = 10			Le = 1000		
ξ	$Nt = 0.1$	$Nt = 0.3$	$Nt = 0.5$	$Nt = 0.1$	$Nt = 0.3$	$Nt = 0.5$
0	0.0687	0.0496	0.0310	0.0676	0.0465	0.0261
0.1	0.1060	0.0862	0.0668	0.1048	0.0828	0.0615
1	0.3227	0.2988	0.2755	0.3208	0.2937	0.2675
10	0.6275	0.5989	0.5711	0.6244	0.5905	0.5579
∞	0.7007	0.6712	0.6423	0.6974	0.6618	0.6277

Table 10 Values of $Nu_{x^*}/Ra_{x^*}^{1/(2n)}$ for various values of ξ, Ω, and A^* with $Nr = Nb = 0.5$, $Nt = 0.2$, Le = 5, $R_d = 2$, $H = 1.5$, $n = 0.5$

	$Nu_{x^*}/Ra_{x^*}^{1/(2n)}$					
	$\Omega = 0$			$\Omega = 0.5$		
ξ	$A^* = 0$	$A^* = 0.5$	$A^* = 1$	$A^* = 0$	$A^* = 0.5$	$A^* = 1$
0	1.0736	0.6652	0.2585	1.6184	1.2480	0.8808
0.1	1.1242	0.7178	0.3131	1.6948	1.3260	0.9603
1	1.4051	1.0110	0.6188	2.1181	1.7605	1.4062
10	1.7734	1.3988	1.0262	2.6734	2.3371	2.0042
∞	1.8594	1.4897	1.1221	2.8029	2.4725	2.1454

Lewis number Le (Le = 10, 1000), respectively, with $Nr = Nb = 0.5$, $R_d = 0.5$, $H = 1.2$, $A^* = 1$, $n = 1$, $\Omega = 0.5$, $\xi = 0.1$. In Fig. 4, for the fixed Le, increasing the thermophoresis parameter Nt widens the dimensionless temperature profile and narrows the dimensionless wall temperature gradient. This occurs because the thermophoresis force generated by the temperature gradient moves the fluid fast away from the surface. Therefore, the nanoparticles from the hot surface are driven toward the ambient, which has a larger effect on the fluid and causes a larger dimensionless temperature profile. However, for the given Nt, the dimensionless wall temperature gradient slightly decreases when the Lewis number Le increases. In Fig. 5, it is apparent when Nt increases or Le decreases, dimensionless nanoparticle volume fraction profile increases.

Table 9 lists the local Nusselt number $Nu_{x^*}/Ra_{x^*}^{1/(2n)}$ for various values of ξ, Le, and Nt with $Nr = Nb = 0.5$, $R_d = 0.5$, $H = 1.2$, $A^* = 1$, $n = 1$, $\Omega = 0.5$. Results show that for the fixed ξ and Le, increasing the thermophoresis parameter Nt reduces the local Nusselt number. Figure 4 shows that this occurs because the increase in the thermophoresis parameter tends to decrease the dimensionless wall temperature gradient, which reduces the local Nusselt number. Besides, for the given ξ and Nt, as the Lewis number Le is enhanced, the local Nusselt number a little decreases.

Figures 6 and 7 present the effects of two values of the viscosity parameter Ω ($\Omega = 0, 0.5$) and the internal heat generation coefficient A^* ($A^* = 0, 1$) on the dimensionless temperature profile and the dimensionless nanoparticle volume fraction profile with $Nr = Nb = 0.5$, $Nt = 0.2$, Le = 5, $R_d = 2$, $H = 1.5$, $n = 0.5$, $\xi = 10$, respectively. Figure 6 shows that increasing the viscosity parameter or decreasing the internal heat generation coefficient enhances the dimensionless wall temperature gradient. Figure 7 illustrates that the dimensionless wall nanoparticle volume fraction enhances with an increase in the viscosity parameter or a decrease in the internal heat generation coefficient.

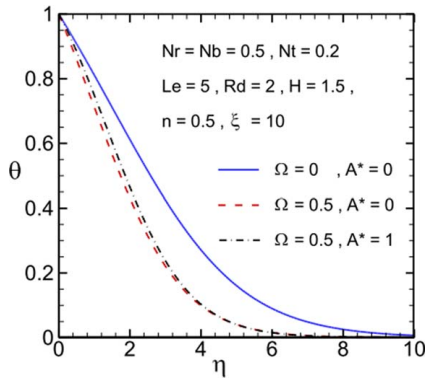

Fig. 6 Dimensionless temperature profile for two values of Ω and A^*

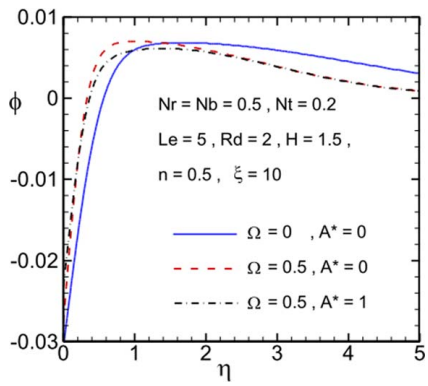

Fig. 7 Dimensionless nanoparticle volume fraction profile for two values of Ω and A^*

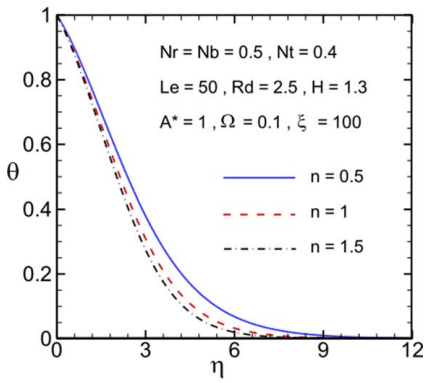

Fig. 8 Dimensionless temperature profile for three values of n

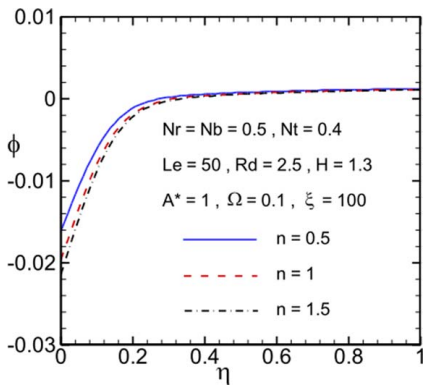

Fig. 9 Dimensionless nanoparticle volume fraction profile for three values of n

Table 11 Values of $Nu_{x^*}/Ra_{x^*}^{1/(2n)}$ for various values of ξ and n with $Nr = Nb = 0.5$, $Nt = 0.4$, $Le = 50$, $R_d = 2.5$, $H = 1.3$, $A^* = 1$, $\Omega = 0.1$

	$Nu_{x^*}/Ra_{x^*}^{1/(2n)}$				
ξ	$n = 0.5$	$n = 0.8$	$n = 1$	$n = 1.2$	$n = 1.5$
0	0.2901	0.3594	0.3863	0.4115	0.4377
0.1	0.3449	0.4178	0.4467	0.4732	0.5008
1	0.6526	0.7458	0.7860	0.8189	0.8549
10	1.0648	1.1847	1.2388	1.2805	1.3274
∞	1.1620	1.2881	1.3452	1.3890	1.4383

Table 10 lists the values of the local Nusselt number $Nu_{x^*}/Ra_{x^*}^{1/(2n)}$ for various values of ξ, Ω, and A^* with $Nr = Nb = 0.5$, $Nt = 0.2$, $Le = 5$, $R_d = 2$, $H = 1.5$, $n = 0.5$. First, when ξ and A^* are fixed, as the viscosity parameter Ω is enhanced, the local Nusselt number increases. This occurs because enhancing the viscosity parameter tends to decrease the viscosity of the fluid, thus accelerating the velocity of fluid and increasing the local Nusselt number. Second, when ξ and Ω are fixed, the local Nusselt number tends to decrease when the internal heat generation coefficient A^* increases. Increasing the internal heat generation coefficient increases the thermal boundary layer thickness, as revealed in Fig. 6. As the thermal boundary layer thickness increase, the local Nusselt number decreases.

Figures 8 and 9 illustrate the dimensionless temperature profile and the dimensionless nanoparticle volume fraction profile for three values of the power-law index n ($n = 0.5$, 1, and 1.5) with $Nr = Nb = 0.5$, $Nt = 0.4$, $Le = 50$, $R_d = 2.5$, $H = 1.3$, $A^* = 1$, $\Omega = 0.1$, $\xi = 100$, respectively. Figure 8 shows that increasing the power-law index causes both the dimensionless temperature profile and the thermal boundary thickness to become thin, and thus enhancing the dimensionless wall temperature gradient. However, Fig. 9 shows that an increase in the power-law index decreases the dimensionless nanoparticle volume fraction profile.

Table 11 gives the values of the local Nusselt number $Nu_{x^*}/Ra_{x^*}^{1/(2n)}$ for various values of ξ and n with $Nr = Nb = 0.5$, $Nt = 0.4$, $Le = 50$, $R_d = 2.5$, $H = 1.3$, $A^* = 1$, $\Omega = 0.1$. The table indicates that, for the fixed ξ, enhancing the power-law index n tends to increase the local Nusselt number because an increase in the power-law index tends to reduce the thermal boundary layer thickness, as shown in Fig. 8. As the thinner the thermal boundary layer thickness decreases, the local Nusselt number increases.

Conclusions

A steady, two-dimensional, laminar boundary layer analysis was performed to study the effect of zero nanoparticles flux (ZNF) on natural convection over an isothermal vertical truncated cone embedded in Darcy porous media filled with a nanofluid. Thermophoresis and Brownian motion effects are also considered. After the coordinate transformation is performed, the transformed governing equations are obtained and solved by KBM. Comparisons with previously published work revealed good agreement. The numerical analysis results of present study are summarized as follows:

(1) The local Nusselt number increases with increasing the radiation parameter R_d, the surface temperature parameter H, and the dimensionless streamwise coordinate ξ.
(2) Increasing the thermophoresis parameter Nt and the Lewis number Le reduces the local Nusselt number.
(3) Increasing the viscosity parameter Ω increases the local Nusselt number. However, enhancing the internal heat generation coefficient A^* has tendency to decrease the local Nusselt number.
(4) Enhancing the power-law index n tends to increase the local Nusselt number.

Conflict of Interest

There are no conflicts of interest.

Data Availability Statement

The datasets generated and supporting the findings of this article are obtainable from the corresponding author upon reasonable request. The authors attest that all data for this study are included in the paper.

Nomenclature

c = specific heat at constant pressure
d = particle diameter
f = dimensionless stream function
g = gravitational acceleration
k = equivalent thermal conductivity
r = local radius of the vertical truncated cone
u = velocity in the x-direction
v = velocity in the y-direction
x = streamwise coordinate
y = transverse coordinate
C = nanoparticle volume fraction
H = surface temperature parameter
T = temperature of fluid
a_r = Rosseland mean extinction coefficient
h_{x^*} = local convective heat transfer coefficient
x_o = distance of the leading edge of vertical truncated cone measured from the origin
D_B = Brownian diffusion coefficient
D_T = thermophoretic diffusion coefficient
R_d = radiation parameter
q''' = internal heat generation rate per unit volume
x^* = distance measured from the leading edge of the vertical truncated cone
A^* = internal heat generation coefficient
$K(n)$ = modified permeability of the porous medium
Le = Lewis number
Nb = Brownian motion parameter
Nr = buoyancy ratio
Nt = thermophoresis parameter
Nu_{x^*} = local Nusselt number
Ra_{x^*} = local Rayleigh number

Greek Symbols

α = equivalent thermal diffusivity
β = volumetric expansion coefficient
γ = half angle of the vertical truncated cone
ε = porosity
η = pseudo-similarity variable
θ = dimensionless temperature
μ = viscosity of fluid
ξ = dimensionless streamwise coordinate
ρ_f = fluid density
ρ_p = nanoparticle mass density
$(\rho c)_f$ = heat capacity of the fluid
$(\rho c)_p$ = heat capacity of nanoparticle material
σ_o = Stefan–Boltzmann constant
σ_s = scattering coefficient
τ = heat capacity ratio between nanoparticle and fluid
φ = dimensionless nanoparticle volume fraction
ψ = stream function
Ω = viscosity parameter

Subscripts

w = condition at the wall
∞ = ambient

References

[1] Nield, D. A., and Bejan, A., 2017, *Convection in Porous Media*, Springer, New York.
[2] Cheng, P., Le, T. T., and Pop, I., 1985, "Natural Convection of a Darcian Fluid About a Cone," Int. Commun. Heat Mass, **12**(6), pp. 705–717.
[3] Chamkha, A. J., 1996, "Non-Darcy Hydromagnetic Free Convection From a Cone and a Wedge in Porous Media," Int. Commun. Heat Mass, **23**(6), pp. 875–887.
[4] Chamkha, A. J., Bercea, C., and Pop, I., 2006, "Free Convection Flow Over a Truncated Cone Embedded in a Porous Medium Saturated with Pure or Saline Water at low Temperatures," Mech. Res. Commun., **33**(4), pp. 433–440.
[5] Yih, K. A., 1999, "Coupled Heat and Mass Transfer by Free Convection Over a Truncated Cone in Porous Media: VWT/VWC or VHF/VMF," Acta Mech., **137**(1–2), pp. 83–97.
[6] Cheng, C. Y., 2000, "An Integral Approach for Heat and Mass Transfer by Natural Convection From Truncated Cones in Porous Media: With Variable Wall Temperature and Concentration," Int. Commun. Heat Mass, **27**(4), pp. 537–548.
[7] Takhar, H. S., Chamkha, A. J., and Nath, G., 2000, "Combined Heat and Mass Transfer Along a Vertical Moving Cylinder With a Free Stream," Heat Mass Transfer, **36**(3), pp. 237–246.
[8] Chamkha, A. J., and Khaled, A.-R. A., 2000, "Hydromagnetic Combined Heat and Mass Transfer by Natural Convection From a Permeable Surface Embedded in a Fluid-Saturated Porous Medium," Int. J. Numer. Methods Heat Fluid Flow, **10**(5), pp. 455–477.
[9] Takhar, H. S., Chamkha, A. J., and Nath, G., 2003, "Unsteady Mixed Convection Flow From a Rotating Vertical Cone With a Magnetic Field," Heat Mass Transfer, **39**(4), pp. 297–304.
[10] Cheng, C. Y., 2010, "Soret and Dufour Effects on Heat and Mass Transfer by Natural Convection From a Vertical Truncated Cone in a Fluid-Saturated Porous Medium With Variable Wall Temperature and Concentration," Int. Commun. Heat Mass, **37**(8), pp. 1031–1035.
[11] Chen, H. T., and Chen, C. K., 1988, "Free Convection Flow of Non-Newtonian Fluids Along a Vertical Plate in a Porous Medium," J. Heat Trans-T ASME, **110**(1), pp. 257–260.
[12] Wang, C. Y., and Tu, C. J., 1989, "Boundary-Layer Flow and Heat Transfer of Non-Newtonian Fluids in Porous Media," Int. J. Heat Fluid Fl., **10**(2), pp. 160–165.
[13] Yih, K. A., 1998, "Uniform Lateral Mass Flux Effect on Natural Convection of Non-Newtonian Fluids Over a Cone in Porous Media," Int. Commun. Heat Mass, **25**(7), pp. 959–968.
[14] Cheng, C. Y., 2009, "Natural Convection Heat Transfer of Non-Newtonian Fluids in Porous Media From a Vertical Cone Under Mixed Thermal Boundary Conditions," Int. Commun. Heat Mass, **36**(7), pp. 693–697.
[15] Cheng, C. Y., 2009, "Natural Convection Heat and Mass Transfer From a Vertical Truncated Cone in a Porous Medium Saturated With a Non-Newtonian Fluid With Variable Wall Temperature and Concentration," Int. Commun. Heat Mass, **36**(6), pp. 585–589.
[16] Groşan, T., and Pop, I., 2001, "Free Convection Over a Vertical Flat Plate with a Variable Wall Temperature and Internal Heat Generation in a Porous Medium Saturated With a Non-Newtonian Fluid," Tech. Mech., **21**(4), pp. 313–318.
[17] Groşan, T., Postelnicu, A., and Pop, I., 2004, "Free Convection Boundary Layer Over a Vertical Cone in a Non-Newtonian Fluid Saturated Porous Medium With Internal Heat Generation," Tech. Mech., **24**(2), pp. 91–104.
[18] Chamkha, A. J., and Al-Mudhaf, A., 2005, "Unsteady Heat and Mass Transfer From a Rotating Vertical Cone With a Magnetic Field and Heat Generation or Absorption Effects," Int. J. Therm. Sci., **44**(3), pp. 267–276.
[19] Al-Mudhaf, A., and Chamkha, A. J., 2005, "Similarity Solutions for MHD Thermosolutal Marangoni Convection Over a Flat Surface in the Presence of Heat Generation or Absorption Effects," Heat Mass Transfer, **42**(2), pp. 112–121.
[20] Chamkha, A. J., Al-Mudhaf, A. F., and Pop, I., 2006, "Effect of Heat Generation or Absorption on Thermophoretic Free Convection Boundary Layer From a Vertical Flat Plate Embedded in a Porous Medium," Int. Commun. Heat Mass, **33**(9), pp. 1096–1102.
[21] Damseh, R. A., Al-Odat, M. Q., Chamkha, A. J., and Shannak, B. A., 2009, "Combined Effect of Heat Generation or Absorption and First-Order Chemical Reaction on Micropolar Fluid Flows Over a Uniformly Stretched Permeable Surface," Int. J. Therm. Sci., **48**(8), pp. 1658–1663.
[22] Khedr, M.-E. M., Chamkha, A. J., and Bayomi, M., 2009, "MHD Flow of a Micropolar Fluid Past a Stretched Permeable Surface With Heat Generation or Absorption," Nonlinear Anal-Model., **14**(1), pp. 27–40.
[23] Magyari, E., and Chamkha, A. J., 2010, "Combined Effect of Heat Generation or Absorption and First-Order Chemical Reaction on Micropolar Fluid Flows Over a Uniformly Stretched Permeable Surface: The Full Analytical Solution," Int. J. Therm. Sci., **49**(9), pp. 1821–1828.
[24] Rashidi, M. M., and Rastegari, M. T., 2012, "Analytical Solution for Free Convection Boundary-Layer Over a Vertical Cone in a Non-Newtonian Fluid Saturated Porous Medium With Internal Heat Generation," World Appl. Sci. J., **16**, pp. 64–74.
[25] Yih, K. A., and Huang, C. J., 2015, "Effect of Internal Heat Generation on Free Convection Heat and Mass Transfer of Non-Newtonian Fluids Flow Over a Vertical Plate in Porous Media: VWT/VWC," J. Aero. Astro. Avi., **47**, pp. 115–122.
[26] Yih, K. A., and Huang, C. J., 2015, "Effect of Internal Heat Generation on Free Convection Flow of Non-Newtonian Fluids Over a Vertical Truncated Cone in Porous Media: VWT/VWC," J. Air Force Inst. Tech., **14**, pp. 1–18.
[27] Huang, C. J., 2018, "Effects of Internal Heat Generation and Soret/Dufour on Natural Convection of Non-Newtonian Fluids Over a Vertical Permeable Cone in a Porous Medium," J. King Saud Univ.–Sci., **30**(1), pp. 106–111.
[28] Chamkha, A. J., 1997, "Solar Radiation Assisted Convection in Uniform Porous Medium Supported by a Vertical Flat Plate," J. Heat Trans-T ASME, **119**(1), pp. 89–96.
[29] Chamkha, A. J., 2001, "Coupled Heat and Mass Transfer by Natural Convection About a Truncated Cone in the Presence of Magnetic Field and Radiation Effects," Numer. Heat Transfer, Part A, **39**(5), pp. 511–530.
[30] Chamkha, A. J., Mohamed, R. A., and Ahmed, S. E., 2011, "Unsteady MHD Natural Convection From a Heated Vertical Porous Plate in a Micropolar Fluid With Joule Heating, Chemical Reaction and Radiation Effects," Meccanica, **46**(2), pp. 399–411.
[31] Yih, K. A., 2001, "Radiation Effect on Mixed Convection Over an Isothermal Cone in Porous Media," Heat Mass Transfer, **37**(1), pp. 53–57.
[32] Mahmoud, M. A. A., 2012, "Radiation Effect on Free Convection of a Non-Newtonian Fluid Over a Vertical Cone Embedded in a Porous Medium With Heat Generation," ASME J. Appl. Mech. Tech. Phy., **53**(5), pp. 743–750.
[33] Huang, C. J., 2017, "Soret/Dufour Effects on Coupled Heat and Mass Transfer by Free Convection Over a Vertical Permeable Cone in Porous Media With Internal Heat Generation and Thermal Radiation," Heat Transfer Res., **48**(13), pp. 1–14.
[34] Huang, C. J., 2017, "Influence of Uniform Blowing/Suction on the Free Convection of Non-Newtonian Fluids Over a Vertical Cone in Porous Media With Thermal Radiation and Soret/Dufour Effects: UWT/UWC," J. Heat Trans-T ASME, **139**(3), p. 032501.
[35] Gary, J., Kassoy, D. R., Tadjeran, H., and Zebib, A., 1982, "The Effects of Significant Viscosity Variation on Convective Heat Transfer Transport in Water-Saturated Porous Medium," J. Fluid Mech., **117**, pp. 233–249.
[36] Bagai, S., 2004, "Effect of Variable Viscosity on Free Convection Over a Nonisothermal Axisymmetric Body in a Porous Medium With Internal Heat Generation," Acta Mech., **169**(1-4), pp. 187–197.
[37] Kairi, R. R., Murthy, P. V. S. N., and Ng, C. O., 2011, "Effect of Viscous Dissipation on Natural Convection in a Non-Darcy Porous Medium Saturated With Non-Newtonian Fluid of Variable Viscosity," Open Transport Phenom. J., **3**(1), pp. 1–8.
[38] Bagai, S., and Nishad, C., 2012, "Effect of Variable Viscosity on Free Convective Heat Transfer Over a Non-Isothermal Body of Arbitrary Shape in a Non-Newtonian Fluid Saturated Porous Medium With Internal Heat Generation," Transport Porous Med., **94**(1), pp. 277–288.
[39] Achemlal, D., Sriti, M., Haroui, M. E., and Guedda, M., 2014, "Viscosity and Fluid Suction/Injection Effects on Free Convection Flow From a Vertical Plate in a Porous Medium Saturated With a Pseudoplastic Fluid," Int. J. Nonlin. Sci., **18**(2), pp. 127–138.
[40] Cheng, C. Y., 2009, "Nonsimilar Boundary Layer Analysis of Double-Diffusive Convection From a Vertical Truncated Cone in a Porous Medium With Variable Viscosity," Appl. Math. Comput., **212**(1), pp. 185–193.
[41] Mahdy, A., Chamkha, A. J., and Baba, Y., 2010, "Double-diffusive Convection With Variable Viscosity From a Vertical Truncated Cone in Porous Media in the Presence of Magnetic Field and Radiation Effects," Comput. Math. Appl., **59**(12), pp. 3867–3878.
[42] Narayana, M., Khidir, A. A., Sibanda, P., and Murthy, P. V. S. N., 2013, "Soret Effect on the Natural Convection From a Vertical Plate in a Thermally Stratified Porous Medium Saturated With Non-Newtonian Liquid," J. Heat Trans-T ASME, **135**(3), p. 032501.
[43] Buongiorno, J., 2006, "Convective Transport in Nanofluids," J. Heat Trans-T ASME, **128**(3), pp. 240–250.
[44] Kakaç, S., and Pramuanjaroenkij, A., 2009, "Review of Convective Heat Transfer Enhancement With Nanofluids," Int. J. Heat Mass Transfer, **52**(13–14), pp. 3187–3196.
[45] Mahdi, R. A., Mohammed, H. A., Munisamy, K. M., and Saeid, N. H., 2015, "Review of Convection Heat Transfer and Fluid Flow in Porous Media With Nanofluid," Renewable Sustainable Energy Rev., **41**, pp. 715–734.
[46] Nield, D. A., and Kuznetsov, A. V., 2009, "The Cheng-Minkowycz Problem for Natural Convective Boundary-Layer Flow in a Porous Medium Saturated by a Nanofluid," Int. J. Heat Mass Transfer, **52**(25–26), pp. 5792–5795.
[47] Cheng, C. Y., 2012, "Natural Convection Boundary Layer Flow Over a Truncated Cone in a Porous Medium Saturated by a Nanofluid," Int. Commun. Heat Mass, **39**(2), pp. 231–235.
[48] Cheng, C. Y., 2012, "Free Convection of Non-Newtonian Nanofluids About a Vertical Truncated Cone in a Porous Medium," Int. Commun. Heat Mass, **39**(9), pp. 1348–1353.
[49] Rashad, A. M., EL-Hakiem, M. A., and Abdou, M. M. M., 2011, "Natural Convection Boundary Layer of a Non-Newtonian Fluid About a Permeable Vertical Cone Embedded in a Porous Medium Saturated WITH a Nanofluid," Comput. Math. Appl., **62**(8), pp. 3140–3151.
[50] Hady, F. M., Ibrahim, F. S., Abdel-Gaied, S. M., and Eid, M. R., 2011, "Effect of Heat Generation/Absorption on Natural Convective Boundary-Layer Flow From a Vertical Cone Embedded in a Porous Medium Filled With a Non-Newtonian Nanofluid," Int. Commun. Heat Mass, **38**(10), pp. 1414–1420.
[51] Chamkha, A. J., Rashad, A. M., RamReddy, C., and Murthy, P. V. S. N., 2014, "Effect of Suction/Injection on Free Convection Along a Vertical Plate in a Nanofluid Saturated Non-Darcy Porous Medium With Internal Heat Generation," Indian J. Pure Ap. Mat., **45**(3), pp. 321–341.
[52] Chamkha, A. J., Abbasbandy, S., Rashad, A. M., and Vajravelu, K., 2013, "Radiation Effects on Mixed Convection About a Cone Embedded in a Porous Medium Filled With a Nanofluid," Meccanica, **48**(2), pp. 275–285.
[53] Khan, W. A., Makinde, O. D., and Khan, Z. H., 2016, "Non-aligned MHD Stagnation Point Flow of Variable Viscosity Nanofluids Past a Stretching Sheet With Radiative Heat," Int. J. Heat Mass Transfer, **96**, pp. 525–534.

[54] Kuznetsov, A. V., and Nield, D. A., 2013, "The Cheng–Minkowycz Problem for Natural Convective Boundary Layer Flow in a Porous Medium Saturated by a Nanofluid: A Revised Model," Int. J. Heat Mass Transfer, **65**, pp. 682–685.
[55] Cheng, C. Y., 2014, "Analysis of Free Convection About a Vertical Cone in a Porous Medium Saturated by a Nanofluid," J. Chin. Soc. Mech. Eng., **35**(6), pp. 455–462.
[56] Khan, M., and Khan, W. A., 2016, "MHD Boundary Layer Flow of a Power-Law Nanofluid With New Mass Flux Condition," AIP Adv., **6**(2), p. 025211.
[57] Khan, Z. H., Culham, J. R., Khan, W. A., and Pop, I., 2015, "Triple Convective-Diffusion Boundary Layer Along a Vertical Flat Plate in a Porous Medium Saturated by a Water-Based Nanofluid," Int. J. Therm. Sci., **90**, pp. 53–61.
[58] Kameswaran, P. K., Vasu, B., Murthy, P. V. S. N., and Gorla, R. S. R., 2016, "Mixed Convection From a Wavy Surface Embedded in a Thermally Stratified Nanofluid Saturated Porous Medium With Non-Linear Boussinesq Approximation," Int. Commun. Heat Mass, **77**, pp. 78–86.
[59] Gorla, R. S. R., and Chamkha, A. J., 2011, "Natural Convective Boundary Layer Flow Over a Nonisothermal Vertical Plate Embedded in a Porous Medium Saturated With a Nanofluid," Nanosc. Microsc. Therm., **15**(2), pp. 81–94.
[60] RamReddy, C., Murthy, P. V. S. N., Chamkha, A. J., and Rashad, A. M., 2013, "Soret Effect on Mixed Convection Flow in a Nanofluid Under Convective Boundary Condition," Int. J. Heat and Mass Transfer, **64**, pp. 384–392.
[61] Ghalambaz, M., Behseresht, A., Behseresht, J., and Chamkha, A. J., 2015, "Effects of Nanoparticles Diameter and Concentration on Natural Convection of the Al_2O_3–Water Nanofluids Considering Variable Thermal Conductivity Around a Vertical Cone in Porous Media," Adv. Powder Technol., **26**(1), pp. 224–235.
[62] Sudarsana Reddy, P., and Chamkha, A. J., 2016, "Soret and Dufour Effects on MHD Convective Flow of Al_2O_3–Water and TiO_2–Water Nanofluids Past a Stretching Sheet in Porous Media With Heat Generation/Absorption," Adv. Powder Technol., **27**(4), pp. 1207–1218.
[63] Reddy, P. S., Sreedevia, P., and Chamkha, A. J., 2017, "MHD Boundary Layer Flow, Heat and Mass Transfer Analysis Over a Rotating Disk Through Porous Medium Saturated by Cu-Water and Ag-Water Nanofluid with Chemical Reaction," Powder Technol., **307**(1), pp. 46–55.
[64] Rasool, G., Zhang, T., Chamkha, A. J., Shafiq, A., Tlili, I., and Shahzadi, G., 2020, "Entropy Generation and Consequences of Binary Chemical Reaction on MHD Darcy-Forchheimer Williamson Nanofluid Flow Over non-Linearly Stretching Surface," Entropy, **22**(1), p. 18.
[65] Christopher, R. V., and Middleman, S., 1965, "Power-Law Flow Through a Packed Tube," Ind. Eng. Chem. Fundam., **4**(4), pp. 424–426.
[66] Dharmadhirkari, R. V., and Kale, D. D., 1985, "Flow of Non-Newtonian Fluids Through Porous Media," Chem. Eng. Sci., **40**(3), pp. 527–529.
[67] Cebeci, T., and Bradshaw, P., 1984, *Physical and Computational Aspects of Convective Heat Transfer*, Springer, New York.